Pergamon

Int. J. Solids Structures Vol. 35, No. 19, pp. 2457–2473, 1998

0020–7683/98 $19.00 + .00

PII: S0020–7683(97)00149–2

MICROMECHANICAL MODELING OF MARTENSITIC TRANSFORMATION IN RANDOM MICROSTRUCTURES*

G. REISNER, E. A. WERNER and F. D. FISCHER
Institute of Mechanics and Institute of Metal Physics, Montanuniversität Leoben, 8700 Leoben, Austria

(*Received* 19 *May* 1997)

Abstract—A thermodynamic transformation criterion is used to describe the strain induced martensitic transformation (SIMT) in two different materials, namely in a dilute Cu–Fe alloy and in a low alloyed TRIP-steel. A finite element calculation makes it possible to evaluate the local stress and strain fields and to monitor the kinetics of the martensitic transformation. The degree of randomness of the austenite's crystallographic lattice orientation with respect to an external load direction strongly influences the stability of the austenite against SIMT. The effect of the austenite grain size on its stability against SIMT and on the microstructure of the martensite is investigated.

1. INTRODUCTION

By exploiting the TRIP (Transformation Induced Plasticity) phenomenon in low alloyed dual phase steels it became possible recently to obtain deep drawing steels with both increased strength and ductility (Matsumura *et al.*, 1987). The strain induced martensitic transformation (SIMT) is responsible for an extraordinary work hardening of the material by delaying the onset of strain localisation during plastic deformation. The occurrence of the TRIP effect is mainly determined by the stability of the austenite against martensitic transformation. Several influencing factors have been identified like the size of the transforming region, its chemical composition, the spatial arrangement and the crystallographic orientation of the austenite (Rigsbee, 1980; Reisner *et al.*, 1996).

In this paper the influence of the degree of randomness of the austenite's orientation with respect to an external loading direction on the stability of the austenite against SIMT will be addressed. Two very different materials/microstructures will be considered, namely a dilute Cu–Fe-alloy containing very small austenite particles and a low alloyed TRIP-steel which possesses austenitic inclusions that are typically an order of magnitude larger than those in the Cu–Fe-alloys. In a dilute Cu–2% Fe alloy the austenitic iron precipitates transform into martensite exhibiting a microstructure consisting of parallel plates (bands) of martensite (Kato *et al.*, 1976; Monzen *et al.*, 1981; Easterling and Weatherly, 1969; Ishida and Kiritani, 1988). Describing this discrete transformation process layer by layer with a model formulated at the micro-scale allows to investigate the influence of the randomness of the lattice orientation on the SIMT incorporating features such as the particle size and the number of bands formed in each particle.

For low alloyed TRIP-steels the SIMT can be described using a meso-scale model, in which the austenite grain can be treated as continuum, since the number of discrete bands of martensite is very large. This approach makes possible to study the influence of the texture of the austenitic grains on their transformation behavior by assigning crystallographic orientations to the individual grains and by studying the interactions of several inclusions in the course of the transformation.

For both materials (microstructures) a thermodynamics transformation criterion is used in this work to predict the onset and/or the kinetics of the transformation. The

* Dedicated to Professor Franz Ziegler on the occasion of his 60th birthday.

criterion is implemented into the finite element code ABAQUS with the purpose to study the transformation by monitoring the local stress and strain fields introduced into the materials by the SIMT (Hibbit *et al.*, 1995).

2. TRANSFORMATION CRITERION

A transformation criterion (TC) compares the value of a certain state function after the transformation with its initial value. In the case of an irreversible process in a solid the state function itself becomes a functional. With an explicit expression for a state functional one is able to evaluate it for the whole specimen and hence one is able to formulate a so-called global transformation criterion. Due to the history dependence of the actual state it is difficult to identify a state functional. However, there exist some solutions for special materials (e.g. shape memory alloys) (Ball and James, 1987; Roitburd, 1978; Kosenko *et al.*, 1977).

The martensitic transformation in iron or steels causes a considerable volume and shape change. The chemical composition determines the amount of volume dilatation δ. Since δ ranges from 2 to 4%, the volume change due to the martensitic transformation can only be accommodated by plastic flow of the material that surrounds the transforming region. Among other reasons (e.g. low mobility of interfaces due to dissipative processes), this plastification is responsible for the irreversibility of the martensitic transformation in Fe-alloys.

An alternative approach to the global transformation criterion is to state a local transformation criterion (LTC). In this case the LTC predicts a martensitic transformation only if the actual thermodynamic driving force on a phase boundary [see Eshelby (1970)] exceeds a critical value (transformation barrier). This type of LTC is derived by use of the equations of conservation of mass, momentum and energy, the kinematic relations and the second law of thermodynamics. Since the derivation of such a LTC is beyond the scope of this report, we apply a LTC proposed by Fischer (1997) for the transformation of a certain microregion V_μ:

$$\int_{V_\mu} \sigma|_0 : \varepsilon^{\mathrm{T}}\,\mathrm{d}V + \int_{V_\mu} \rho\Delta\varphi_{\mathrm{chem}}\,\mathrm{d}V = F_{\mathrm{c}} + \Delta\Gamma + \int_V \int_0^t \tau : \dot{\varepsilon}^{\mathrm{pl}}\,\mathrm{d}\tilde{t}\,\mathrm{d}V + \frac{1}{2}\int_V \tau : \mathbf{L}^{-1} : \tau\,\mathrm{d}V, \quad (1)$$

where $\mathbf{L}$ is the elasticity tensor. The local stress state at the beginning of the transformation $\sigma|_0$ can be expressed as the sum of the external stress state Σ and an internal stress state σ^{int} due to the stress redistribution caused by the microstructure. τ is an additional internal stress state that represents the stress fluctuation introduced by the martensitic transformation of V_μ (i.e. $\tau|_0 = 0$):

$$\sigma|_0 = \Sigma + \sigma^{\mathrm{int}}, \quad \sigma|_t = \Sigma + \sigma^{\mathrm{int}} + \tau, \quad \int_V \sigma^{\mathrm{int}}\,\mathrm{d}V = \int_V \tau\,\mathrm{d}V = 0. \quad (2)$$

The stress free transformation strain ε^{T} is only present in the transforming microregion V_μ. Although the integral of the internal stress state τ over the whole volume vanishes, $\int_{V_\mu} \sigma : \varepsilon^{\mathrm{T}}\,\mathrm{d}V$ takes on a finite value over the transforming region. We call this entity the mechanical driving force (MDF). Patel and Cohen (1953) introduced the term mechanical driving force already 40 years ago in their pioneering work. However, in their terminology the MDF is the product of the external stress state with the stress free transformation strain (MDF $= \Sigma : \varepsilon^{\mathrm{T}}$). The chemical driving force (CDF) is understood as the difference of the chemical energy of the stress free phases austenite and martensite, $\Delta\varphi_{\mathrm{chem}}$, weighted by the density ρ integrated over the transforming region V_μ.

The terms on the right-hand side of eqn (1) represent different contributions to the transformation barrier. $\Delta\Gamma$ stands for the change in energy due to the newly formed interfaces. It is interesting to note that not the total plastic dissipation ($\int_V \int_0^t \sigma : \dot{\varepsilon}^{\mathrm{pl}}\,\mathrm{d}\tilde{t}\,\mathrm{d}V$)

due to the martensitic transformation acts as restricting force, but only the plastic dissipation due to the fluctuation of the stress state (τ). This part of the plastic dissipation $\int_V \int_0^t \tau : \dot{\varepsilon}^{pl} \, d\tilde{t} \, dV$ will be referred to as W_{pl}^{τ}. The integration with respect to time in the above expression of W_{pl}^{τ} indicates the path dependence of the plastic dissipation. The transformation of the microregion V_μ takes place in the time range from 0 to t. However, t has no physical meaning in our simulation, since inertia forces are not considered.

Similarly to the plastic dissipation, only the elastic strain energy $W_{el}^{\tau} = \frac{1}{2}\int_V \tau : \mathbf{L}^{-1} : \tau \, dV$ due to τ enters the transformation barrier. W_{pl}^{τ} and W_{el}^{τ} are calculated by integration over the volume of the whole specimen and are, therefore, nonlocal entities reflecting the contributions of the nontransforming material surrounding V_μ to the transformation barrier. Finally, F_c denotes all contributions to the transformation barrier that have not been identified yet (e.g. the energy of the internal interfaces within the martensite).

To facilitate the comparison of the LTC for varying volume fractions of newly formed martensite, V_μ, we recast eqn (1) by using energy densities instead:

$$\mathrm{MDF}' + \mathrm{CDF}' = F_c' + \Delta\Gamma' + (W_{pl}^{\tau})' + (W_{el}^{\tau})', \tag{3}$$

where X' denotes the density of entity X, i.e. its specific value per unit volume of transforming material. It is important to note that the interface energy density $\Delta\Gamma' = \Delta\Gamma / V_\mu$ is defined by the interface energy per unit volume of newly formed martensite. A specific interface energy (i.e. energy per unit area of interface) will be denoted by $\gamma_{\alpha\beta}$, where α and β stand for the neighboring phases.

This kind of LTC necessitates the access to local stresses and strains which can be achieved by using the finite element method. The commercially available code ABAQUS allows for a subroutine in which the material behavior can be coded by the user (UMAT) (Hibbit *et al.*, 1995). In this user defined routine the local stress state is decomposed into Σ, σ^{int} and τ in each material point, so that all stress dependent terms in eqn (1) may be evaluated. A detailed discussion of the other entities of eqn (1) and of their evaluation is given in the following sections separately for each material.

3 SIMT IN A DILUTE Cu–Fe ALLOY

3.1. *Geometrical and material model*

The fcc Fe-particles are precipitated in a spherical shape during an annealing treatment from a supersaturated Cu–Fe mono- or polycrystal (Kato *et al.*, 1976; Monzen *et al.*, 1981; Easterling and Weatherly, 1969; Ishida and Kiritani, 1988). Therefore, Fe-precipitates are homogeneously distributed within the Cu–Fe alloy and almost no clustering of the particles is observed. The size of the particles varies; excellent micrographs of such particles can be found in the paper by Kato *et al.* (1976). Particles with a radius less than 10 nm are fully coherent with the Cu-matrix. If the radius is larger than 10 nm, coherency is lost and the particles become semi-coherent or fully incoherent (Li *et al.*, 1985). The lattice mismatch between the particle and the matrix is accommodated by interfacial misfit dislocations, which, due to their presence, reduce the coherency strains (Matthews, 1979).

For our simulation we choose a representative volume element (RVE) with a single austenitic inclusion embedded in a Cu-matrix. The volume fraction of the inclusion is 2%. For the sake of simplicity we consider a thin slab of the alloy so that the part of the spherical inclusion inside the RVE can be approximated by a cylinder. To account for this simplification of the geometry, generalized plane strain conditions are prescribed parallel to the normal of the slab (i.e. the axis of the cylinder) (Hibbit *et al.*, 1995). Assuming a hexagonal pattern of inclusions, the slab can be divided into hexagonal prisms each with a Fe-precipitate in its center (Fig. 1). Periodic boundary conditions are enforced on the surface of the unit cell.

The cylinder is divided into several parallel slabs of identical thickness. Each layer corresponds to a martensite band. As depicted in Fig. 1 direction 1 is parallel and direction 2 is normal to the interface of two neighboring martensite bands. The numbers of martensite

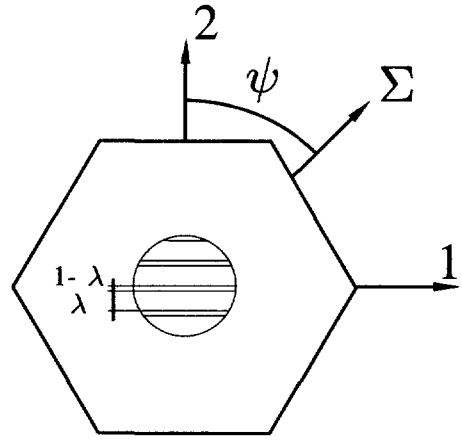

Fig. 1. Sketch of the representative volume element (RVE) of the Cu–Fe alloy. The volume fraction of the fcc Fe-precipitate is 2% and the number of martensite bands is 8. The austenite inclusion is exaggerated in size. The direction 3 is out of plane. The applied force Σ for the simulation of the tensile test and the compression test acts in the 1–2 plane. ψ denotes the angle between the direction of Σ and direction 2.

bands and particles sizes modeled are $N \in (1, 2, 3, 4, 6, 8, 12, 24)$ and $r \in (15, 25, 40, 60\ \text{nm})$, respectively.

We consider two distinct loading cases, namely a uniaxial tensile test and a single pass cold rolling process. In both cases the applied force acts in the transverse plane (i.e. the plane given by directions 1 and 2) of the RVE. ψ denotes the angle between the applied load and direction 2. The single pass cold rolling process is modeled by a plane strain compressive test. To account for the plane deformation in the rolling process the displacement in direction 3 is constrained.

The smallest transformable volume is a single layer. If the TC given by eqn (3) is fulfilled in a certain layer, the martensitic transformation is simulated by attaching the stress free transformation strain ε^T to V_μ. During the transformation the external load is held constant. Following the phenomenological theory of the martensitic transformation by Wechsler *et al.* (1953) (WLR), ε^T can be determined solely from the lattice parameters of the parent and the product phase. The lattice parameter a_0 of the fcc parent phase austenite is 0.361 nm. Due to the small amount of Cu solved in the Fe-precipitate, the product phase martensite shows a bct lattice with a ratio of tetragonality of $c/a \simeq 1.1$ (lattice parameters $a = 0.28$ and $c = 0.31$ nm) (Denny, 1956).

With this input data the stress free transformation strain is determined as:

$$\varepsilon^T = \begin{bmatrix} 0 & \pm 0.078 & 0 \\ \pm 0.078 & 0.036 & 0 \\ 0 & 0 & 0 \end{bmatrix}. \tag{4}$$

The WLR theory states that ε^T is an invariant plane strain. In our model ε^T acts in the transverse plane given by directions 1 and 2. The macroscopically undistorted plane between austenite and martensite, called the habit plane, is normal to direction 2. The volume dilatation of 3.6% is achieved by an expansion normal to the habit plane, only. The shear deformation of $\gamma_0 = 2\varepsilon^T_{12} = 0.156$ acts in the 1–2 plane. Neighboring layers of martensite shear into opposite directions as indicated by the $\pm\varepsilon^T_{12}$ in eqn (4).

The Fe-precipitates in the Cu-matrix cause a considerable hardening due to the Orowan mechanism (Biselli and Morris, 1994). A standard continuum mechanical model is not able to capture the Orowan mechanism which is based on the movement of a single dislocation. Thus, similar to a self consistent approach the experimental flow curve of a Cu–2% Fe alloy with a mean Fe-particle diameter of 40 nm as reported by Tiefenthaler *et al.* (1995) is assigned to the Cu-matrix.

Table 1. Material input data for the numerical simulation of SIMT in a dilute Cu–2%Fe alloy. A Ludwik-type of flow behavior is assumed. Σ_0 denotes the yield strength. K and n are hardening parameters and ν is the Poisson's ratio

Phase	Σ_0 [MPa]	K [GPa]	n	ν	Youngs modulus [GPa]
Copper	120	432	0.46	0.28	130
Austenite	200	300	0.60	0.3	210
Martensite	400	150	0.80	0.3	210

For all phases a von Mises-flow theory (J_2-plasticity), isotropic hardening and a Ludwik-type of hardening behavior are assumed (Ludwik, 1909):

$$\Sigma = \Sigma_0 + K\varphi^n. \tag{5}$$

The material input data are summarized in Table 1. While there is a marked difference in the strength of martensite and austenite, we assume that the flow behavior of the single crystal Fe-precipitates in both, austenitic and martensitic states, does not change with the particle size. For a given volume fraction of precipitated Fe-particles the interparticular spacing depends on the number of Fe-precipitates and thus on the mean size of the precipitates. The interparticular spacing in turn determines the increase in yield strength by the Orowan mechanism. Although the hardening of the Cu-matrix by iron precipitates is large, the difference in the contributions of this hardening mechanism to the total yield strength in Cu–Fe alloys with Fe-particles sized in the range of 20–40 nm is less than 20 MPa at a total strength level of 120 MPa (Tiefenthaler, 1995). Therefore, the flow curve for a particle size of 40 nm is taken as representative for all particle sizes in the range of 30–120 nm so that the particle size enters the model only via $\Delta\Gamma'$.

3.2. *Estimation of the transformation barrier for the Cu–Fe alloy*

The phase transformation causes new interfaces to appear and hence changes the specific energy of the Fe–Cu interface:

$$\Delta\Gamma = A^{\alpha'\gamma}\gamma_{\alpha'\gamma} + A^{\mathrm{FeCu}}\Delta\gamma_{\mathrm{FeCu}}, \quad \Delta\gamma_{\mathrm{FeCu}} = \gamma_{\alpha'\varepsilon} - \gamma_{\gamma\varepsilon}. \tag{6}$$

α', γ and ε stand for martensite, austenite and the Cu-matrix, respectively. $A^{\alpha'\gamma}$ denotes the area of the newly formed interface between martensite and austenite (habit plane). A^{FeCu} is the area of the interface between V_μ and the Cu-matrix. $\gamma_{\alpha'\gamma}$, the specific energy of a habit plane, is estimated as 0.02 [N m^{-1}]. This value is larger than the one for a coherent twin plane in austenite ($\gamma_{\gamma\bar{\gamma}}^{\mathrm{TW}} = 0.013$ [N m^{-1}]) and smaller than the one for a $\gamma/\bar{\gamma}$ large angle grain boundary $\gamma_{\gamma\bar{\gamma}}^{\mathrm{GB}}$, which can be estimated as four times as large as $\gamma_{\gamma\bar{\gamma}}^{\mathrm{TW}}$ (Nabarro, 1967; Verhoeven, 1975).

As a first approximation we consider only the change in the specific interface energy inherent in A^{FeCu}, $\Delta\gamma_{\mathrm{FeCu}}$, to contribute to the transformation barrier. The specific energy of a martensite to Cu-matrix interface ($\gamma_{\alpha'\varepsilon}$) is assumed to be 0.2 [N m^{-1}] larger than $\gamma_{\gamma\varepsilon}$, the specific energy of the austenite/copper interface.

$\Delta\Gamma$ depends on the values of $\gamma_{\alpha'\gamma}$ and $\Delta\gamma_{\mathrm{FeCu}}$ and on the geometry (i.e. the particle radius r and the number of martensite bands). Since the area of the interfaces, $A^{\mathrm{FeCu}} + A^{\alpha'\gamma}$, scales with r^2 and V_μ scales with r^3, $\Delta\Gamma'$ is proportional to $1/r$. This is the reason for the importance of $\Delta\Gamma'$ in the transformation barrier for the very small Fe-precipitates in the Cu–Fe alloy. From Fig. 2 one can see that $\Delta\Gamma'$ takes a minimum for $N = 4$, irrespective of the particle size r. Monzen *et al.* investigated a similar dilute Cu–Fe alloy (Monzen *et al.*, 1981). After SIMT they observed twinned Fe-particles with an average band number of 18. An annealing treatment at 673 K caused a diffusional stress relaxation of the inclusion. At the same time, the average number of martensite bands N reduced rapidly within the first few minutes and

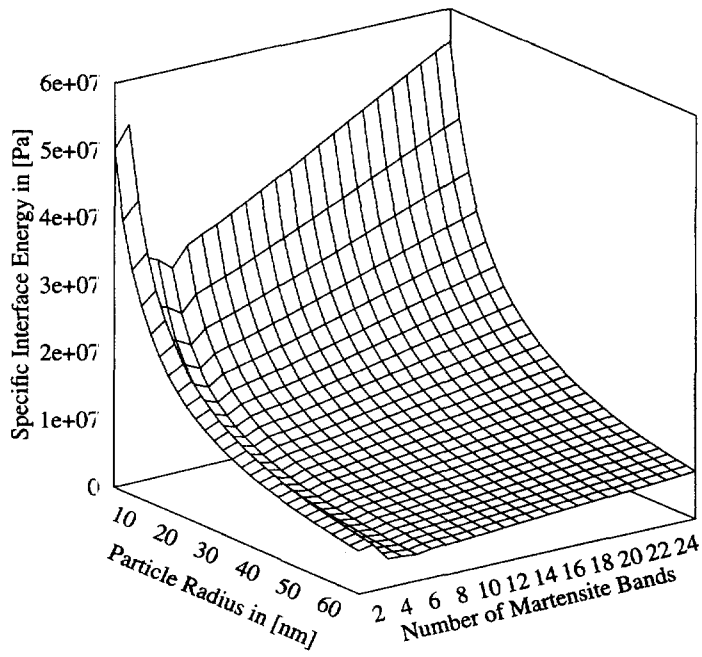

Fig. 2. Interface energy $\Delta\Gamma'$ per unit volume of the transforming material as a function of the particle radius r and the number of martensite bands N. Irrespective of the particle size a microstructure with four martensite bands exhibits the lowest contribution to the transformation barrier.

then remained nearly constant. After annealing 300 min at 673 K the average number of bands observed was 4.

The finite element program allows to determine τ and the elastic and the plastic strain increments in each point so that $(W^{\tau}_{el})'$ and $(W^{\tau}_{pl})'$ can be calculated. $(W^{\tau}_{el})'$ and $(W^{\tau}_{pl})'$ are determined from numerical simulations in which the transformation of a single layer is modeled at constant Σ for all geometries considered. For a given N, the martensitic transformation of layers situated near the axis of the cylinder (inclusion) give approximately the same value for $(W^{\tau}_{pl})'$, whereas for layers near to the surface of the cylinder (with respect to direction 2), $(W^{\tau}_{pl})'$ increases. $(W^{\tau}_{el})'$ is relatively small as compared to $(W^{\tau}_{pl})'$ and is thus neglected. Figure 3 shows $(W^{\tau}_{pl})'$ as a function of N and the equivalent external stress Σ. Forming many martensitic twin bands reduces the overall shape change of the inclusion and thus necessitates less plastic accommodation. $(W^{\tau}_{pl})'$ depends on Σ, since the hardening behavior of the materials is nonlinear (i.e. the higher Σ is, the smaller is the stress increase due to ε^{T} and hence also $(W^{\tau}_{pl})'$).

The stability of the Fe-precipitates in a Cu-matrix against SIMT depends on the particle size. The martensite start temperature M_s can be regarded as a measure for this stability. Li *et al.* (1985) reported that particles of typically several hundred nanometers in diameter loose their stability at room temperature (300 K) and transform to martensite without any external load. However, smaller precipitates, even if they are completely incoherent with the Cu-matrix, remain austenitic at room temperature (Li *et al.*, 1985). Applying the LTC given by eqn (3) for the case that particles of radius $R \approx 250$ nm transform at room temperature in the absence of an applied load ($MDF' = 0$) we find:

$$CDF' = F'_c + (\Delta\Gamma' + (W^{\tau}_{pl})')|_{R \approx 250\,nm}. \tag{7}$$

In the following, we assume that CDF′ and F'_c do not change with the particle size. At room temperature SIMT will occur in particles with $r < R$, if the mechanical driving force and the difference in the transformation barriers for the two particle sizes r and R are the same:

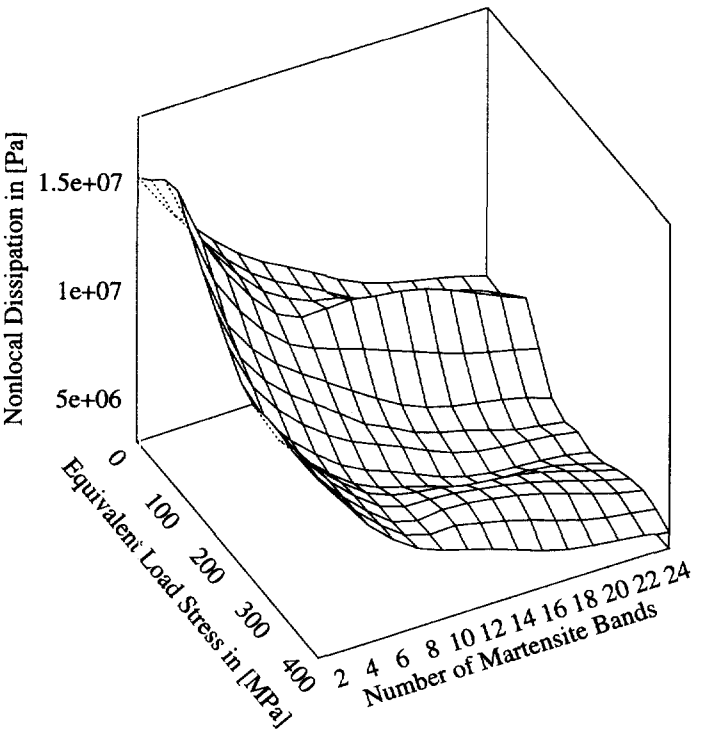

Fig. 3. Nonlocal plastic dissipation $(W_{\mathrm{pl}}^{\tau})'$ due to the stress fluctuations τ caused by SIMT of the first layer that transforms as function of the external stress Σ and the number of martensite bands. With increasing number of martensite bands the overall shape change is reduced so that there is less need for a plastic accommodation in the surrounding matrix.

$$\mathrm{MDF}'|_{300\,\mathrm{K}} = (\Delta\Gamma' + (W_{\mathrm{pl}}^{\tau})')|_{r} - (\Delta\Gamma' + (W_{\mathrm{pl}}^{\tau})')|_{R\approx 250\,\mathrm{nm}}. \tag{8}$$

3.3. *Results and discussion*

Irrespective of the particle size and the number of bands the transformation starts in one of the layers situated near the axis of the cylinder. If the load is not applied parallel to the habit plane normal ($\psi \neq 0$), the direction of the shear component of ε^{T} determines which of the two bands in the center of the cylinder transforms first. For bands of identical thickness these two bands posses the largest relative volume. This maximum in V_{μ} causes a minimum in the contribution of the interface energy to the transformation barrier ($\Delta\Gamma'$). Since the external load, Σ, remains constant during the transformation of a single layer, several layers may transform at the same value of Σ. The transformation of a layer alters the local stress state via the fluctuation stress τ, and the LTC may be fulfilled for another layer, although the external load remains constant. However, irrespective of the loading case inclusions with $N \geqslant 2$ are not transformed at once. The kinetics of SIMT is depicted in Fig. 4 for tensile and compressive loading. The relative volume content of austenite V_{V}^{γ} decreases as the SIMT progresses with increasing plastic strain. For plane strain compression, the austenite possesses a higher stability against SIMT than for tensile loading. At least in the early stages of SIMT there is an excellent agreement of the predicted transformation kinetics with the experimental transformation behavior as reported by Tiefenthaler *et al.* (1995). For both loading types 24 martensite bands are modeled. The particles size in the simulation is $R = 25$ nm, the mean diameter of the particles in the experiments by Tiefenthaler *et al.* (1995) is 40 nm.

Figure 5 shows the equivalent tensile stress necessary to trigger the martensitic transformation of the first layer, $\sigma_{\mathrm{eq.}}^{\mathrm{S}}$, as function of ψ, the angle between the tensile load direction and the habit plane normal. Here, the total number of bands is eight and the particle sizes

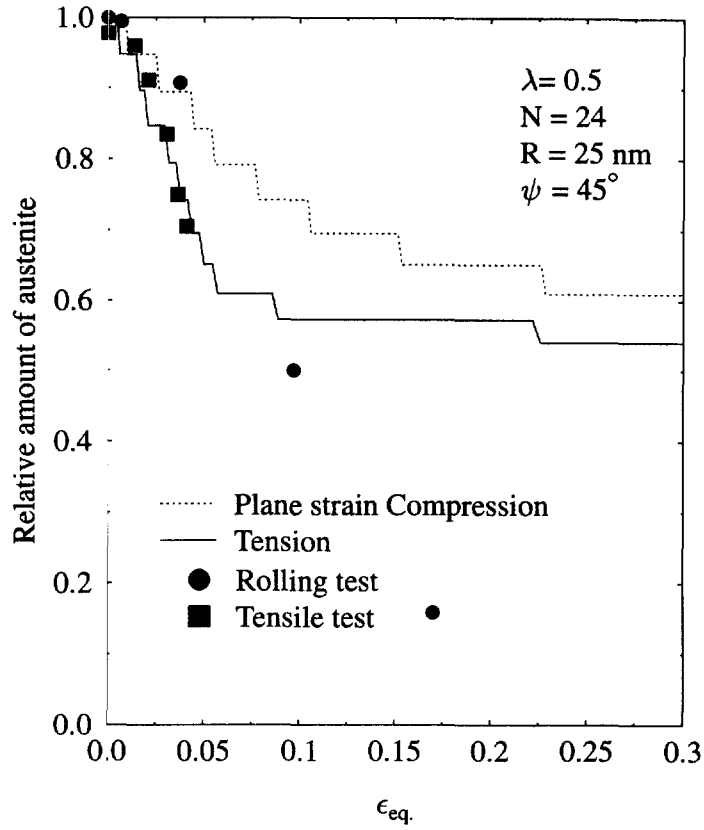

Fig. 4. Transformation kinetics for tensile and compressive loading as predicted numerically and observed experimentally. For both loading types, 24 martensite bands and a particle radius of 25 nm are modeled. The rolling experiment is simulated by a plane strain compression test. At least for the first stage of deformation the kinetics of the SIMT is well described by the numerical model.

are 25 and 40 nm. ψ has a marked influence on the stability against SIMT. For $\psi \simeq 45°$, $\sigma^{S}_{eq.}$ takes on the smallest value, since in this case the shear stress promoting the SIMT is maximal. Due to the transformation strain in the direction 2 and the associated volume dilatation, the variation of $\sigma^{S}_{eq.}$ is not symmetric about $\psi = 45°$. For the plane strain compressive loading the same geometry is simulated. In this case the values of $\sigma^{S}_{eq.}$ are larger than the ones for tensile loading (Fig. 6). This load type sensitivity stems from the positive volume dilatation associated with the martensitic transformation.

This simple model and the use of the LTC allow to capture the size effect on the stability of the Fe-precipitates against SIMT. Figure 7 shows the experimentally observed number of martensite bands formed in more than 50 Fe-precipitates of diameters from 20 to 110 nm as reported by Kato *et al.* (1976), together with the predictions from our simulations. The most favourable number of bands N for a given particle size is determined by selecting the microstructure with the smallest value of $\sigma^{S}_{eq.}$. In reality, there exists a distribution of lattice orientations of the Fe-precipitates and thus a distribution of ψ. In the simulation we select $\psi = 0$ and 45° as limiting cases. Although SIMT occurs mainly during the plastic deformation as has been confirmed by magnetic measurements by Kato *et al.* (1984), the preparation of a thin foil used as specimens for the transmission electron microscope (TEM) can give rise to SIMT. This is due to the fact that the stability of Fe-precipitates against SIMT is smaller for particles that are close to the surface than of particles in the bulk of a specimen (Li *et al.*, 1985). In the preparation of the TEM foils compressive stresses are exerted on the specimen when reducing its thickness by grinding prior to the electrochemical thinning process. Since SIMT can be initiated by this grinding, we also consider compressive loading in our analysis of the size influence on the number of martensite bands formed in an austenitic grain.

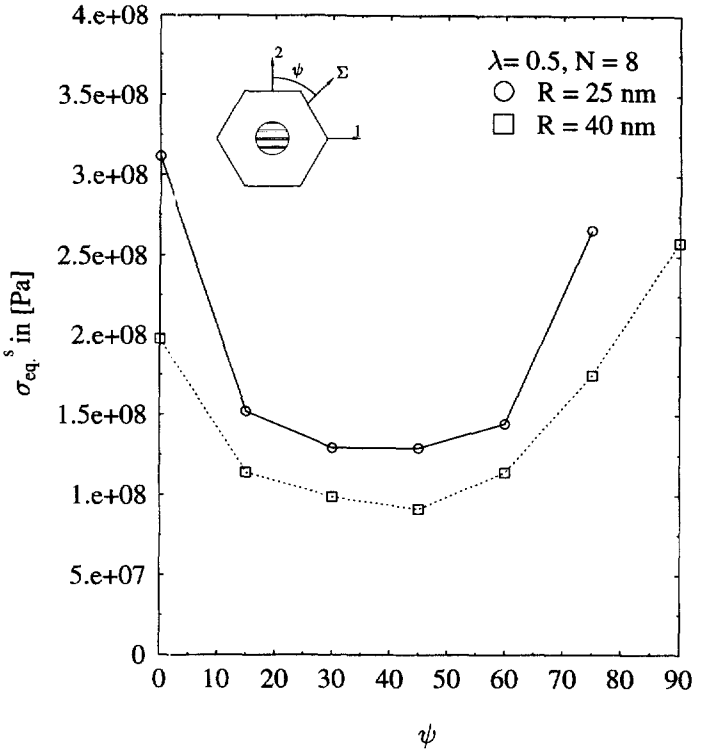

Fig. 5. Necessary stress to start the transformation ($\sigma_{eq.}^{S}$) in the first layer as a function of the angle ψ between the load direction (Σ) and the habit plane normal (direction 2) predicted for tensile loading. Results for two particle sizes (radius 25 and 40 nm) are shown. For both particle sizes the number of martensite bands is eight. Due to the anisotropy of the volume dilatation the curves are not symmetric with respect to $\psi = 45°$.

4. SIMT IN LOW ALLOYED TRIP STEELS

The beneficial effect of the SIMT on the ductility and strength of low alloyed deep drawing steels is due to the impediment to the strain localisation (i.e. necking for tensile specimens) by the additional local hardening caused by the martensitic transformation. For technical applications the transformation of the austenite (retained austenite, RA) should be spread over the whole deformation range rather than occur in a spontaneous manner. Therefore, the gain in ductility and strength of the material depends both on the volume fraction of the RA, V_V^{RA}, and on its stability against SIMT. Besides the local carbon content which determines the CDF′ at a given temperature [see Nishyama (1978)], the crystallographic orientation of the austenite grains with respect to an external loading direction may also influence the stability of the RA against SIMT. The remaining part of this paper tries to shed light on the influence of the lattice orientation (i.e. the texture of the RA-grains) on the transformation behavior for TRIP steels.

4.1. *Microstructure and geometrical model*

The microstructure of a low alloyed TRIP steel is far more complicated than the one of the Cu–Fe alloy. Initially, it consists of the three phases bainite, ferrite and retained austenite (less than 15%) at room temperature. A fourth phase, martensite, evolves as the RA disappears in the course of SIMT. The RA grain size is about 0.5–4.0 μm and the mean diameter about 1–1.5 μm (Jeong *et al.*, 1993). In our micromechanical approach we assume RA grains of constant size and $V_V^{RA} = 10\%$. In the literature, three distinct morphologies of the RA are reported, namely grains embedded in a single ferritic grain (type I), or located at the grain boundary between two or more grains of ferrite (type II), and as thin layer between two bainite regions (type III) (Jeong *et al.*, 1993). In the first two cases the RA grains are of polygonal shape. The thin layers of type III possess a higher stability against

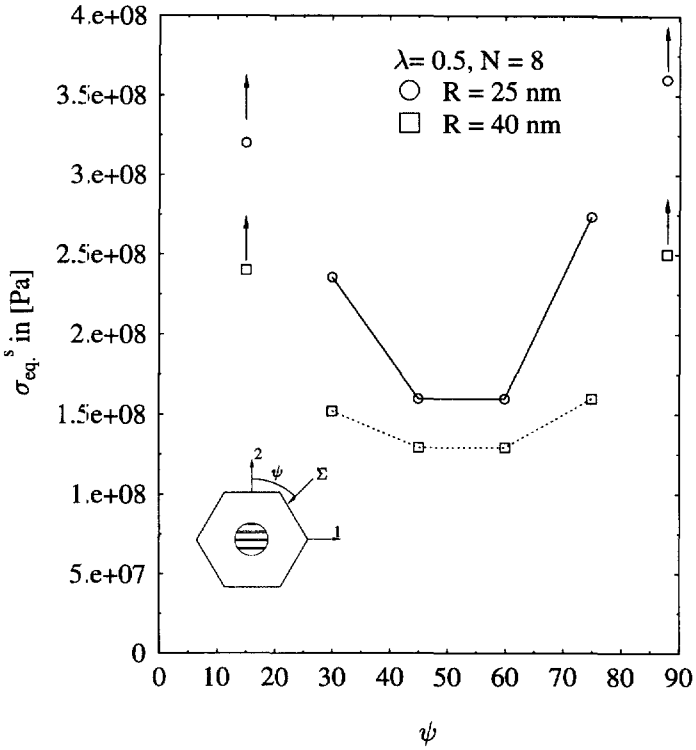

Fig. 6. For plane strain compressive loading $\sigma^S_{eq.}$ is larger than for tensile loading due to the positive volume dilatation. $\sigma^S_{eq.}$ is determined for eight martensite bands and two particles sizes (radius 25 and 40 nm).

SIMT than the two other types and often do not transform at all during deformation of the material (Jeong *et al.*, 1993). Hence, we only consider RA grains of types I and II in our simulations. The microstructure again is idealised by using a unit cell containing 12 grains of RA (Fig. 8). As in the case of the Cu–Fe alloy, a thin slab of the material is modeled by imposing generalized plane strain conditions in direction 3. For the sake of simplicity, the grains are approximated by hexagonal prisms yielding a pseudo two-dimensional microstructure. To study the influence of the texture alone on the kinetics of SIMT, a regular pattern of RA grains is chosen to ensure geometrical symmetry with respect to the external stress state. However, the analysis with the finite element code ABAQUS is performed in a fully three-dimensional way to account for a stress free transformation strain ε^T with components that are not confined to the transverse plane given by directions 1 and 2 (Hibbit *et al.*, 1995). In the user subroutine UMAT, ε^T is an inelastic strain contribution to the total strain ε. In the framework of small strains, ε can be linearly decomposed into an elastic (ε^{el}), a plastic (ε^{pl}) and a transformation strain ε^T.

While the same carbon content is assumed for all RA grains, various lattice orientations may be assigned to the individual grains. On the surface of the hexagonal unit cell periodic boundary conditions are prescribed by enforcing that the displacements of all corresponding nodes on opposing faces of the unit cell differ by a constant displacement vector. Tensile loading is simulated by applying an external force parallel to direction 2 of the RVE.

4.2. *Lattice orientation, texture and* ε^T

In the following a twinned martensite structure with a common undistorted plane, called the habit plane, between itself and the austenite will be referred to as a martensitic variant (Wechsler *et al.*, 1953). Thus, for the cubic to tetragonal phase change, 24 different martensitic variants exist. The amount of the volume dilatation and the shear deformation is the same for all 24 variants. Since in our model all phases are assumed to behave elastically isotropic, the lattice orientation enters the calculations only via the definition of the 24

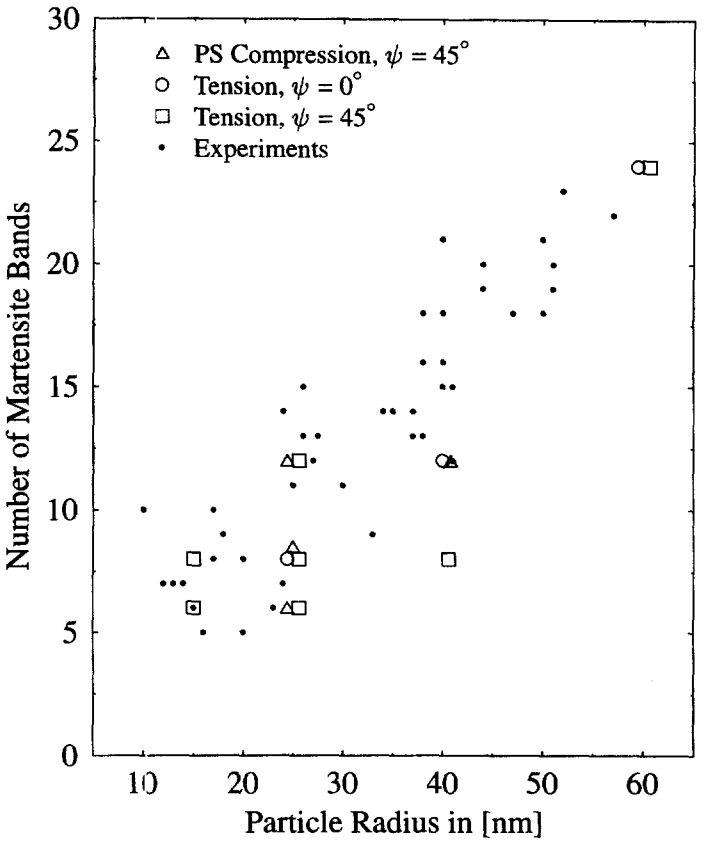

Fig. 7. Size dependence on the number of martensite bands observed in experiments by Kato *et al.* (1976) and predicted by finite element calculations. Tensile and compressive loading cases are considered in the numerical simulation. The lowest stress necessary to start the martensitic transformation determines the number of martensite bands most likely to be formed for a given loading type and particle size.

stress free transformation strains ε_i^T, $i = 1, \ldots, 24$, with respect to the global coordinate system as shown in Fig. 8.

The lattice orientation of the RA grains is given by a set of Eulerian angles defining the misorientation between the local coordinate system of the fcc-RA single crystal and the global coordinate system. In the following the term texture is used to denote a set of 12 Eulerian triplets $(\Omega_1, \ldots, \Omega_{12})$ defining the lattice orientations of the 12 RA grains of the RVE. To study the interaction of several RA grains three types of texture are modeled.

- Sharp texture: all RA grains have the same lattice orientation.
- Mixed (or moderate) texture: only two lattice orientations Ω_1 and Ω_2 are present. The volume fraction relative to the total amount of RA of the grains with orientation Ω_1 is approximately 0.5.
- Random texture: all grains of RA possess different orientation Ω_i, $i = 1, \ldots, 12$.

$\Omega_1, \ldots, \Omega_{12}$ are randomly chosen from a set of more than 2700 triplets of Eulerian angles Ω_i. This set of triplets represents uniformly distributed orientations and it does not contain any pair of triplets of crystallography equivalent lattice orientations (Werner and Prantl, 1988).

To study the influence of the lattice orientation alone, the carbon content is chosen to be 1.3% for all RA grains. This is a reasonable value, since in low alloyed TRIP steels, the austenite contains 1.1–1.7 wt% of carbon (Sugimoto *et al.*, 1992). For 1.3 wt% C the WLR-theory yields a volume dilatation of 2.18% and a shear deformation of 0.144 (Wechsler *et al.*, 1953).

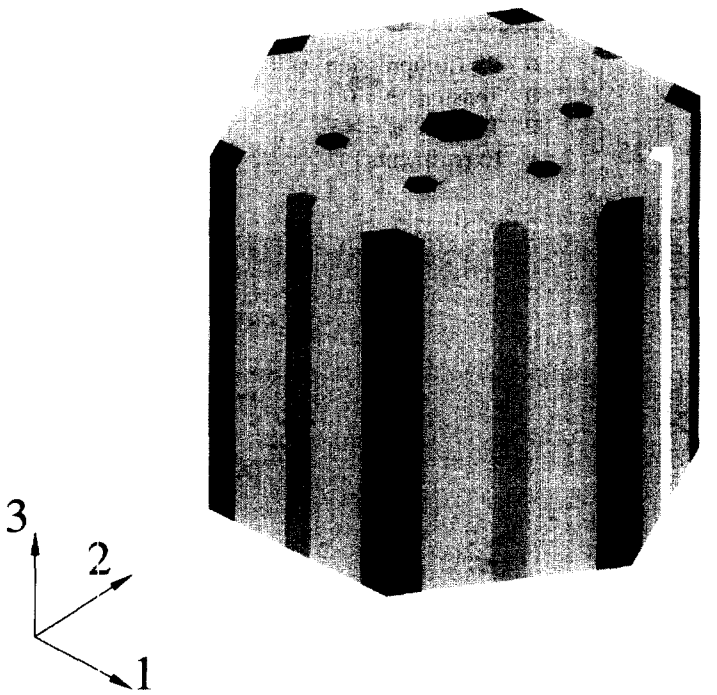

Fig. 8. The representative volume element used in the numerical analysis of SIMT for the low alloyed TRIP steel contains 12 hexagonal grains of RA. The grains at the corners and at the edges of the hexagonal unit cell are divided in three or two parts, respectively. These grains gain their continuity from the periodic boundary conditions enforced on the surface of the RVE.

4.3. *Material model*

Sugimoto *et al.* (1992) report that in low alloyed TRIP steels only parallel layers of martensite are formed by SIMT within a single RA grain. Following this experimental observation we consider only one martensite variant in each RA grain. Since the CDF′ is the same for all 24 possible martensite variants, the variant yielding the largest MDF′ is identified as the active one. Once the martensitic transformation has started, the initially active variant remains active. For the numerical simulation the smallest volume of consideration is the volume V_0 associated with a single integration point, which is used by the finite element code tc evaluate all relevant entities such as stresses and strains. This microregion V_0 consists of austenite containing parallel layers of twinned martensite.

Since the elastic properties of the phases are the same, the martensitic transformation of a band in a single crystal with free surfaces subjected to a dead loading does not change the stress state in both phases. For a crystal embedded in a matrix the martensitic transformation of a band causes different stress states in the austenite and the martensite, although the continuity of tractions along the habit plane imposes some restrictions on the stresses in the two phases. However, at the meso-scale model we assume locally a homogeneous stress state within V_0, the smallest volume of consideration.

The plastic and the transformation strains stored at the integration point correspond to their averaged values over the microregion, respectively. This averaging process over V_0 leads to an incremental formulation of the martensitic transformation. The volume of the newly formed martensite, V_μ, is now given by the increment of martensite per load increment, $\Delta\xi$, instead of being geometrically discretized as it is the case in the study of SIMT in the Cu–Fe alloy. To calculate the amount of transformation in a certain load increment the elastic predictor-radial return method used in J_2-plasticity models is modified (Hibbit *et al.*, 1995). The strain increment associated with the load increment initially is interpreted as an elastic strain increment leading to the total elastic strain ε^{el}_{trial}. The corresponding trial stress state can be either the new stress state at the end of the load increment in the case of an elastic increment or it will be relaxed by martensitic transformation and/or

Table 2. Material input data for the numerical simulation of the SIMT in a low alloyed TRIP steel. Σ_0 denotes the yield strength. K and n are hardening parameters and ν is the Poisson's ratio

Phase	Σ_0 [MPa]	K [MPa]	n	ν	Young's modulus [GPa]
Matrix	300	1000	0.2	0.3	210
Austenite	650	1200	0.4	0.3	210
Martensite	1100	1500	0.5	0.3	210

yielding. The martensitic transformation occurs approximately at one third of the speed of sound and it does not necessitate a dislocation movement (Verhoeven, 1975). Thus, the numerical algorithm considers at first the martensitic transformation to reduce the trial stress state. If the equivalent stress is larger than the actual flow stress, a second radial return occurs by plastic deformation. The MDF at the end of the martensitic transformation for $\Sigma+\Delta\Sigma$ depends on the increment of the volume fraction of martensite per unit volume of austenite, $\Delta\xi'$, formed in the actual load increment:

$$\mathrm{MDF}' = (\varepsilon^{\mathrm{el}}_{\mathrm{trial}} - \Delta\xi'\varepsilon^{\mathrm{T}}) : \mathbf{L} : \varepsilon^{\mathrm{T}}, \tag{9}$$

where it is assumed that only the increment in the transformation strain alters the elastic trial strain state. With $\mathbf{L}$ being the elasticity tensor, $(\varepsilon^{\mathrm{el}}_{\mathrm{trial}} - \Delta\xi'\varepsilon^{\mathrm{T}}) : \mathbf{L}$ denotes the local stress state at the end of the martensitic transformation, but prior to a possible stress relaxation by plastification. On the other hand, the LTC given by eqn (8) has to be fulfilled for the MDF′ at the end of the martensitic transformation at an external load of $\Sigma+\Delta\Sigma$. This leads to a linear expression for $\Delta\xi'$ ensuring that the TC in eqn (8) is not violated at any time. The transformation occurs only in the austenite with an actual relative volume fraction of $(1-\xi)$, where ξ is the relative amount of martensite in the partially transformed RA grain. Hence, the increment of the relative martensitic volume fraction, $\Delta\xi = (1-\xi)\Delta\xi'$, in the considered region V_0 can be written as

$$\Delta\xi = (1-\xi)\frac{\varepsilon^{\mathrm{el}}_{\mathrm{trial}} : \mathbf{L} : \varepsilon^{\mathrm{T}} - (\mathrm{CDF}'|_{M_s} - \mathrm{CDF}'|_{300\,\mathrm{K}})}{\varepsilon^{\mathrm{T}} : \mathbf{L} : \varepsilon^{\mathrm{T}}}. \tag{10}$$

Equivalent to the Cu–Fe alloy, all phases are modeled with an isotropic, Ludwik-type of hardening behavior using J_2-plasticity. The mechanical properties assigned to the matrix phase are chosen to represent a mixture of ferrite and bainite and are similar to those of a ferritic/bainitic steel. For the austenite one has to assume a flow behavior since no austenite with comparable chemical composition (1.3 wt% C) exists as a bulk material at room temperature. The actual flow stress of the transforming particle is calculated from a linear rule of mixture

$$\Sigma_y = (1-\xi)\Sigma_y^{\gamma} + \xi\Sigma_y^{\alpha'} \tag{11}$$

where Σ_y^{γ} and $\Sigma_y^{\alpha'}$ are the flow stresses of retained austenite and martensite, respectively. The material input data are summarized in Table 2.

4.4. *Transformation criterion for TRIP-steels*

For low alloyed TRIP-steels with a mean carbon content of 1.3 wt.% of the RA, room temperature is approximately 80 K above M_s (Andrews, 1965). The CDF′ depends mainly on the temperature and on the chemical composition (carbon content). It consists of a contribution due to the difference in the chemical free energies of the fcc and the bcc crystal structure of pure Fe and of a second part accounting for the role of the carbon content (Kaufman and Cohen, 1958; Nishyama, 1978). To the knowledge of the authors, there are no reports quantifying the influence of the RA grain size on the number N of bands for

low alloyed TRIP-steel. However, N is much larger than for the Cu–Fe alloy, so that even within V_0, which represents a small part of a RA grain, several bands do exist. Thus, we consider that $(W^{\tau}_{pl})'$ and $(W^{\tau}_{el})'$ do not change in the course of SIMT. Since only one grain size of the RA is assumed, $\Delta\Gamma'$ can be treated as constant, too. Thus, at M_s (i.e. MDF′ = 0) we can write

$$\mathrm{CDF}'|_{M_s} = F'_c + \Delta\Gamma' + (W^{\tau}_{pl})' + (W^{\tau}_{el})', \tag{12}$$

and, therefore, the LTC at room temperature for the low alloyed TRIP steel reads:

$$\mathrm{MDF}'|_{300\,\mathrm{K}} = \mathrm{CDF}'|_{M_s} - \mathrm{CDF}'|_{300\,\mathrm{K}}. \tag{13}$$

The value of $\mathrm{CDF}'|_{M_s} - \mathrm{CDF}'|_{300\,\mathrm{K}}$ that enters the model is calculated from Kaufman and Cohen (1958) and Nishyama (1978) as 27.4 MPa.

4.5. *Results and discussion*

For the numerical simulation each RA grain is divided into 36 regions V_0, each of which is associated with an integration point. During the whole SIMT, the deviation of the local relative amount of martensite within a single grain of RA deviates less than 2% from the averaged value taken over the entire grain. Only one active martensite variant is predicted in the entire RA grain at the onset of martensitic transformation. Rao and Rashid (1983) observed directly the SIMT by *in situ* deformation of a low alloyed TRIP steel (0.1% C, 1.5% Mn, 0.5% Si and 0.1% V) in a transmission electron microscope. They found at least two distinct martensite variants in large RA grains. However, in their grains of RA low angle grain boundaries were present separating subgrains with different lattice orientations. Furthermore, much of the constraint by the matrix material is removed in a thin foil specimen, which might not at all behave like the bulk material.

The stability of the RA against SIMT is a consequence of its grain size, its composition and of the constraint imposed by the surrounding matrix (Rigsbee, 1980). In the following we shall address the important role of the texture on the transformation kinetics. Figure 9 shows the relative amount of RA as a function of the equivalent strain in a tensile test. Each curve represents a sharp texture with a distinct lattice orientation Ω_i $i = 1, \ldots, 12$. Denoting the lattice orientation yielding the smallest (largest) relative amount of RA as Ω_{min} (Ω_{max}), Ω_{min} (Ω_{max}) gives the orientation with the lowest (highest) stability against SIMT among all lattice orientations considered. There exists a marked difference in the transformation kinetics for the orientations Ω_{min} and Ω_{max}. Although all grains have the same lattice orientation, the relative amount of the RA varies considerably from grain to grain and different variants are activated in these grains due to the evolving internal stress state.

The dashed and dotted curves in Fig. 10 correspond to the kinetics of the sharp textures Ω_{min} and Ω_{max}, respectively. The solid lines represent three realisations of mixed textures composed of the two lattice orientations Ω_{min} and Ω_{max}. The transformation kinetics is close to that one would expect from a linear rule of mixture of the kinetics for Ω_{min} and Ω_{max}. This is also true for a mixed texture composed of orientations other than Ω_{min} and Ω_{max}. The three cases of the mixed texture are distinguished only by the way Ω_{min} and Ω_{max} are assigned to the 12 RA grains. The volume fractions of grains with Ω_{min} and Ω_{max} are always the same. Hence, the conclusion may be drawn, that the internal stress state governs the stability against SIMT, since the spatial arrangement of the RA grains is the same in all three realisations.

The transformation kinetics for a randomly textured microstructure is quite similar to that of the mixed texture. The solid curves in Fig. 11 correspond to different realisations of a random texture, each composed of 12 different lattice orientations. The deviation in the relative amount of RA between the realisations with the highest and the lowest stability against SIMT is only 15% at an equivalent strain of 20%.

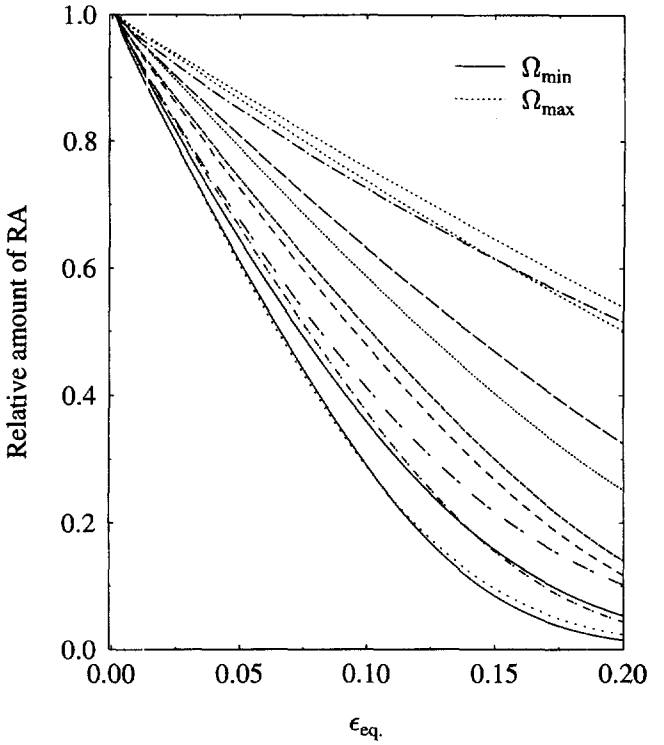

Fig. 9. The relative amount of RA as a function of the equivalent strain in a tensile test. Each curve represents a sharp texture with a distinct lattice orientation Ω_i, $i = 1, \ldots, 12$. Ω_{min} denotes the lattice orientation yielding the smallest relative amount of RA and Ω_{max} the one leading to the largest relative amount of RA.

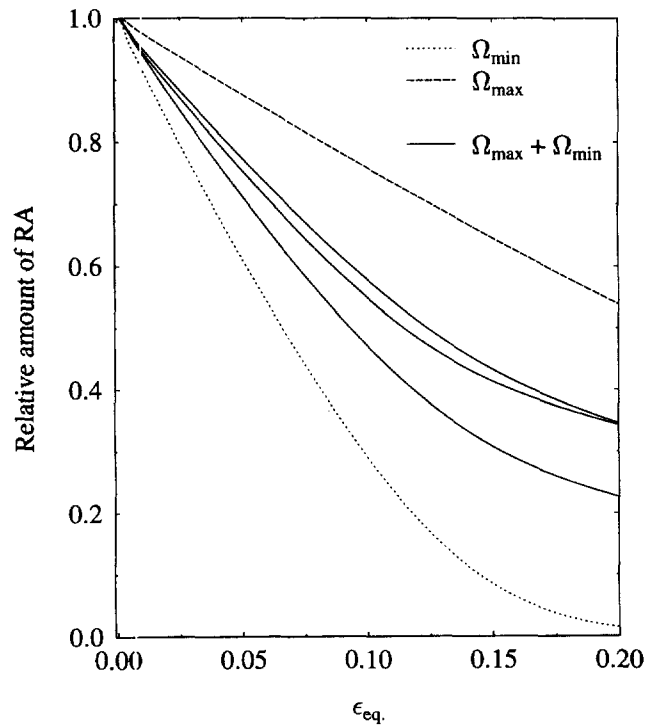

Fig. 10. The dashed and dotted curves correspond to the sharp textures Ω_{min} and Ω_{max}, respectively. The solid curves represent a mixed texture composed of the two lattice orientations Ω_{min} and Ω_{max}. The transformation kinetics is close to that one would expect from a linear rule of mixture of the kinetics for Ω_{min} and Ω_{max}.

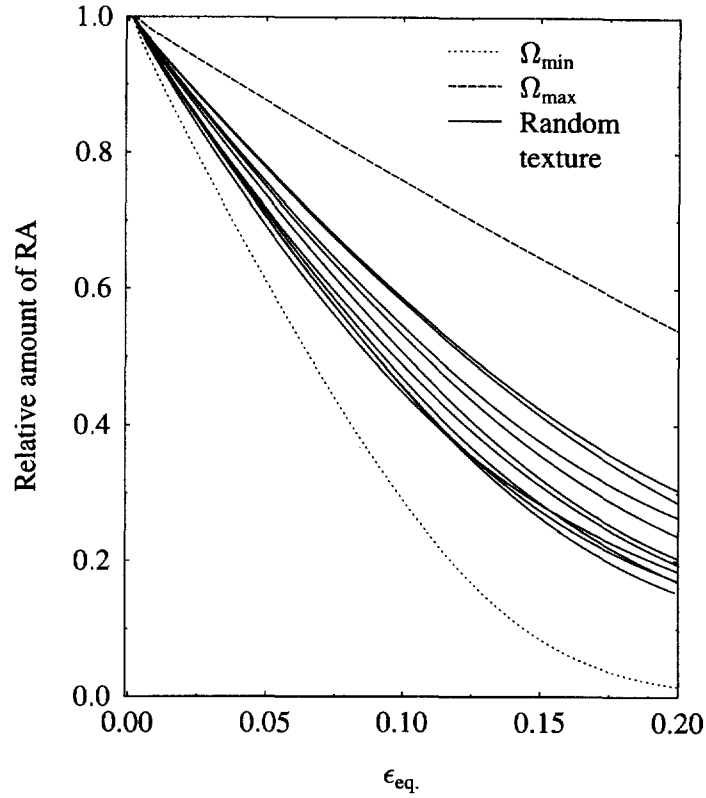

Fig. 11. The solid curves show the kinetics of 10 different realisations of a random texture, each composed of 12 different lattice orientations assigned to the RA grains.

5. CONCLUSIONS

A thermodynamic transformation criterion (TC) proposed recently by Fischer (1997) makes it possible to describe the onset and the kinetics of the strain induced martensitic transformation (SIMT) of austenitic grains. The degree of randomness of the austenite's crystallographic orientation with respect to the external loading direction plays a prominent role for the stability against SIMT. Detailed micromechanical studies of two very different materials (microstructures) reveal the following:

- The transformation of a single martensite band in the austenitic precipitate in the Cu–Fe alloy may initiate the martensitic transformation in the neighboring band.
- The influence of the particle size on the stability of austenite against SIMT is identified to be a function of its microstructure. For the Cu–Fe alloy the number of martensite bands formed by SIMT increases with increasing particle size. This is also predicted by our calculations.
- The stability of austenite against SIMT shows a marked load type sensitivity. The experimental observation, that the austenite is less stable under tensile loading than under compressive loading, is also made when modeling the SIMT for these two loading cases.
- Besides the grain size, the chemical composition and the constraint imposed by the surrounding matrix, the crystallographic orientation of the grains determines the stability of the austenite in low alloyed TRIP steels. The transformation kinetics depends strongly on the type of texture given by the lattice orientations Ω_i of the austenitic inclusions. A high degree of randomness in the lattice orientations yields a transformation kinetics that is close to the average of the transformation kinetics for sharp textures.

REFERENCES

Andrews, K. W. (1965) Empirical formulae for the calculation of some transformation temperatures. *Journal of the Iron and Steel Institute*, July 1965, pp. 721–727.

Ball, J. M. and James, R. D. (1987) Fine phase mixtures as minimizers of energy. *Archiv for Rational Mechanics and Analysis* **100,** 13–52.

Biselli, C. and Morris, D. G. (1994) Microstructure and strength of Cu–Fe *in situ* composites obtained from prealloyed Cu–Fe powders. *Acta Metallurgica et Materialia* **34,** 163–176.

Denney, J. M. (1956) Precipitate kinetics and structure in a Cu–2.4% Fe alloy. *Acta Metalurgica* **4,** 586–592.

Easterling, K. E. and Weatherly, G. C. (1969) On the nucleation of martensite in iron precipitates. *Acta Metallurgica* **17,** 845–852.

Eshelby, J. D. (1970) Energy relations on the energy-momentum tensor in continuum mechanics. In *Inelastic Behavior of Solids*, ed. M. F. Kanninen, W. F. Adler, A. R. Rosenfield and R. I. Joffee. McGraw-Hill, New York.

Fischer, F. D. (1997) Modeling and simulation of transformation induced plasticity in elasto-plastic materials. In *Mechanics of Solids with Phase Changes*. CISM Series, Vol. 368, Springer, Wien, New York.

Hibbit, Karlsson and Sorensen (1995) *ABAQUS Version 5.5, Theory Manual*. Hibbit, Karlson & Sorensen, Pawtucket, RI, U.S.A.

Ishida, I. and Kiritani, M. (1988) The $\gamma \rightarrow \alpha$ transformation mechanism of fine iron precipitates in copper base alloys. *Acta Metallurgica* **36,** 2129–2139.

Jeong, W. C., Matlock, D. K. and Krauss, G. (1993) Observation of deformation and transformation behavior of retained austenite in a 0.14 C–1.2 Si–1.5 Mn steel with ferrite–bainite–austenite structure. *Materials Science and Engineering* **A165,** 1–8.

Kato, M., Monzen, R. and Mori, T. (1976) A stress induced martensitic transformation of spherical iron particles in a Cu–Fe alloy. *Acta Metallurgica* **26,** 605–613.

Kato, M., Toksoy, C., Lee Pak, C. S., Pratt, W. and Mukherjee, K. (1984) Magnetization measurement associated with $\gamma \rightarrow \alpha$ martensitic transformation of Fe particles in a Cu–1.59% Fe alloy. *Metallurgical Transactions A* **15A,** 755–756.

Kaufman, L. and Cohen, M. (1958) The martensitic transformation in the iron–nickel system. *Journal of Metals*, 165–173.

Kosenko, N. S., Roitburd, A. L. and Khandros, L. G. (1977) Thermodynamics and morphology of martensitic transformation under external stress. *Physics of Metals and Metallography* **44,** 956–965.

Li, C. H., Porter, D. A. and Easterling, K. E. (1985) A lattice resolution study of the martensitic transformation of small iron particles in a copper matrix. *Acta Metallurgica* **33,** 317–328.

Ludwik, P. (1909) *Elemente der Technischen Mechanik*. Springer, Berlin.

Matthews, J. W. (1979) Misfit dislocations. In *Dislocations in Solids*, Vol. 2, ed. F. R. N. Nabarro. North-Holland, New York.

Matsumura, O., Sakuma, Y. and Takechi, H. (1987) TRIP and its kinetic aspects in austempered 0.4 C–1.5 Si–0.8 Mn steel. *Scripta Metallurgica* **21,** 1301–1306.

Monzen, R., Kato, M. and Mori, T. (1981) Structural changes of iron particles in a deformed and annealed Cu–Fe alloy single crystal. *Transactions of the Japan Institute of Metals* **37,** 65–73.

Nabarro, F. R. N. (1967) *Theory of Crystal Dislocations*. Oxford University Press, Oxford.

Nishiyama, Z. (1978) *Martenitic Transformations*. Academic Press, New York.

Patel, J. R. and Cohen, M. (1953) Criterion for the action of applied stress in the martensitic transformation. *Acta Metallurgica* **1,** 531–538.

Rao, B. V. N. and Rashid, M. S. (1983) Direct observation of deformation-induced retained austenite transformation in a vanadium-containing dual-phase steel. *Metallography* **16,** 19–37.

Reisner, G., Tiefenthaler, B., Werner, E. and Fischer, F. D. (1996) Strain-induced martensitic transformation in a dilute Cu–Fe alloy—micromechanical modeling and experiments. *Materials Science and Engineering* **A215,** 50–56.

Rigsbee, J. M. (1980) Inhibition of martensitic transformation in small austenitic particles in low alloy steels. In *Proceedings of the ICOMAT 1979*, Cambridge, MA, U.S.A.

Roitburd, A. L. (1978) *Solid State Physcis*, 1st edn. Academic Press, New York.

Sugimoto, K., Kobayashi, M. and Hashimoto, S. (1992) Ductility and strain-induced transformation in a high-strength transformation induced plasticity-aided dual-phase steel. *Metallurgical Transactions A* **23A,** 3085–3091.

Tiefenthaler, B., Reisner, G. and Werner, E. (1995) Verformungsinduzierte Martensitbildung in einer Kupfer–Eisen–Legierung: Experimente und Modellierung. *Zeitschrift für Metallkunde* **86,** 845–851.

Tiefenthaler, B. (1995) Master thesis, Montanuniversität Leoben.

Verhoeven, J. D. (1975) *Fundamentals of Physical Metallurgy*. Wiley, New York.

Wechsler, M. S., Lieberman, D. S. and Read, T. A. (1953) On the theory on the formation of martensite. *Journal of Metals* **197,** 1503–1515.

Werner, E. and Prantl, W. (1988) Statistical treatment of measured orientation relationships in orientation space. *Journal of Applied Crystallography* **21,** 311–316.